BIOCHEMISTRY
including biophysical chemistry & molecular biology

Article

pubs.acs.org/biochemistry

Arg314 Is Essential for Catalysis by *N*-Acetyl Neuraminic Acid Synthase from *Neisseria meningitidis*

Dmitri D. A. Joseph, Wanting Jiao, and Emily J. Parker*

Biomolecular Interaction Centre and Department of Chemistry, University of Canterbury, Christchurch, New Zealand

Supporting Information

ABSTRACT: The sialic acid *N*-acetylneuraminic acid (NANA) has a key role in the pathogenesis of a select number of neuroinvasive bacteria such as *Neisseria meningitidis*. These pathogens coat themselves with polysialic acids, mimicking the exterior surface of mammalian cells and consequentially concealing the bacteria from the host's immune system. NANA is synthesized in bacteria by the homodimeric enzyme NANA synthase (NANAS), which catalyzes a condensation reaction between phosphoenolpyruvate (PEP) and *N*-acetylmannosamine (ManNAc). NANAS is closely related to the α-keto acid synthases 3-deoxy-D-*arabino*-heptulosonate 7-phosphate synthase and 3-deoxy-D-*manno*-octulosonate 8-phosphate synthase. NANAS differs from these enzymes in that it contains an antifreeze protein like (AFPL) domain, which extends from the C-terminal of the $(\beta/\alpha)_8$ barrel containing the active site and contributes a highly conserved arginine (Arg314) into the active site of the opposing monomer chain. We have investigated the role of Arg314 in *Nme*NANAS through mutagenesis and a combination of kinetic and structural analyses. Using isothermal titration calorimetry and molecular modeling, we have shown that Arg314 is required for the catalytic function of NANAS and that the delocalized positively charged guanidinium functionality of this residue provides steering of the sugar substrate ManNAc for suitable placement in the active site and thus reaction with PEP.

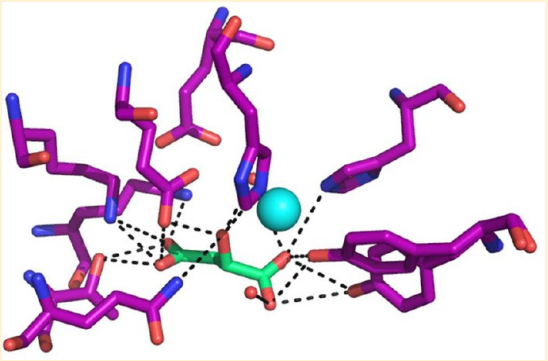

Sialic acids are a structurally diverse family of sugars containing α-keto acid functionalities on a nine-carbon backbone.[1] *N*-Acetylneuraminic acid (NANA) is the most commonly occurring sialic acid in nature, with an *N*-acetyl group at the C5 position.[2] Sialic acids are not ubiquitous in nature despite their diversity,[3] being predominantly present in vertebrates and a few pathogenic bacteria.[2,4] In mammals, these compounds play important roles in cellular recognition and cell adhesion processes and are thus typically incorporated as terminal residues of cell surface glycoconjugates.[5−7] Sialic acids are present in essentially all types of mammalian tissue with the highest concentration being in the central nervous system.[5] In the central nervous system, polysialic acid polymers are present on the neuronal cell adhesion molecule.[6,7]

In prokaryotes, sialic acids have been identified in a select number of pathogenic bacteria such as *Escherichia coli*,[8] *Neisseria meningitidis* (the causative agent of meningitis),[9] and *Campylobacter jejuni* (the causative agent of food-borne gastroenteritis).[10−12] These pathogens produce sialylated capsular polysaccharides, mimicking the exterior surface of mammalian cells and consequentially concealing the bacteria from the host's immune system.[3]

The biosynthesis of NANA occurs via slightly different pathways in mammals and bacteria.[13,14] In mammals, biosynthesis occurs via phosphorylated intermediates, converting *N*-acetyl mannosamine (ManNAc) to ManNAc 6-phosphate (ManNAc-6-P) before condensing MaNAc-6-P with PEP to produce NANA 9-phosphate (NANA9P). NANA9P is finally dephosphorylated to generate NANA. The bacterial biosynthetic pathway bypasses the phosphorylation and dephosphorylation processes of mammalian metabolism and directly condenses ManNAc and PEP using the enzyme *N*-acetylneuraminic acid synthase (NANAS) to produce NANA (Figure 1). The final step in both the mammalian and bacterial pathways is the production of the activated form of sialic acid, CMP-NeuNAc. CMP-NeuNAc is utilized by sialyltransferases to incorporate NeuNAc into glycoproteins and glycolipids.[15]

The structure of *N. meningitidis* NANAS (*Nme*NANAS) (Figure 2) has been previously elucidated (PDB codes 1XUZ and 2WQP).[1,9] The structure has been determined with Mn^{2+}, PEP and a reduced form of ManNAc, *N*-acetylmannosaminitol (rManNAc) bound and has also been determined with a tetrahedral intermediate mimic bound. Both structures have revealed that *Nme*NANAS is a domain swapped homodimer, with each subunit comprising two structurally distinct domains joined by a linker region. The N-terminal domain of *Nme*NANAS is a $(\beta/\alpha)_8$ barrel fold and contributes the majority of the residues comprising the catalytic site. The C-terminal domain comprises 65 amino acid residues and strongly resembles the fold of fish type III antifreeze proteins.[16,17] The antifreeze protein like (AFPL) domain caps the catalytic

Received: January 16, 2013
Revised: March 13, 2013
Published: March 27, 2013

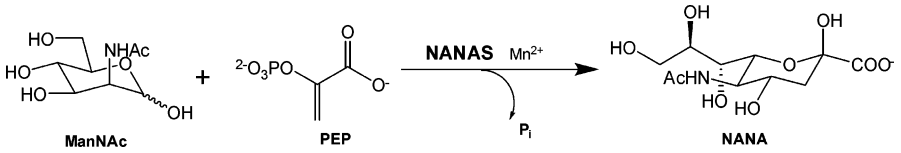

Figure 1. Reaction catalyzed by *N*-acetylneuraminic acid synthase (NANAS). NANAS catalyzes a condensation reaction between phosphoenolpyruvate (PEP) and *N*-acetylmannosamine (ManNAc) to produce *N*-acetylneuraminic acid (NANA).

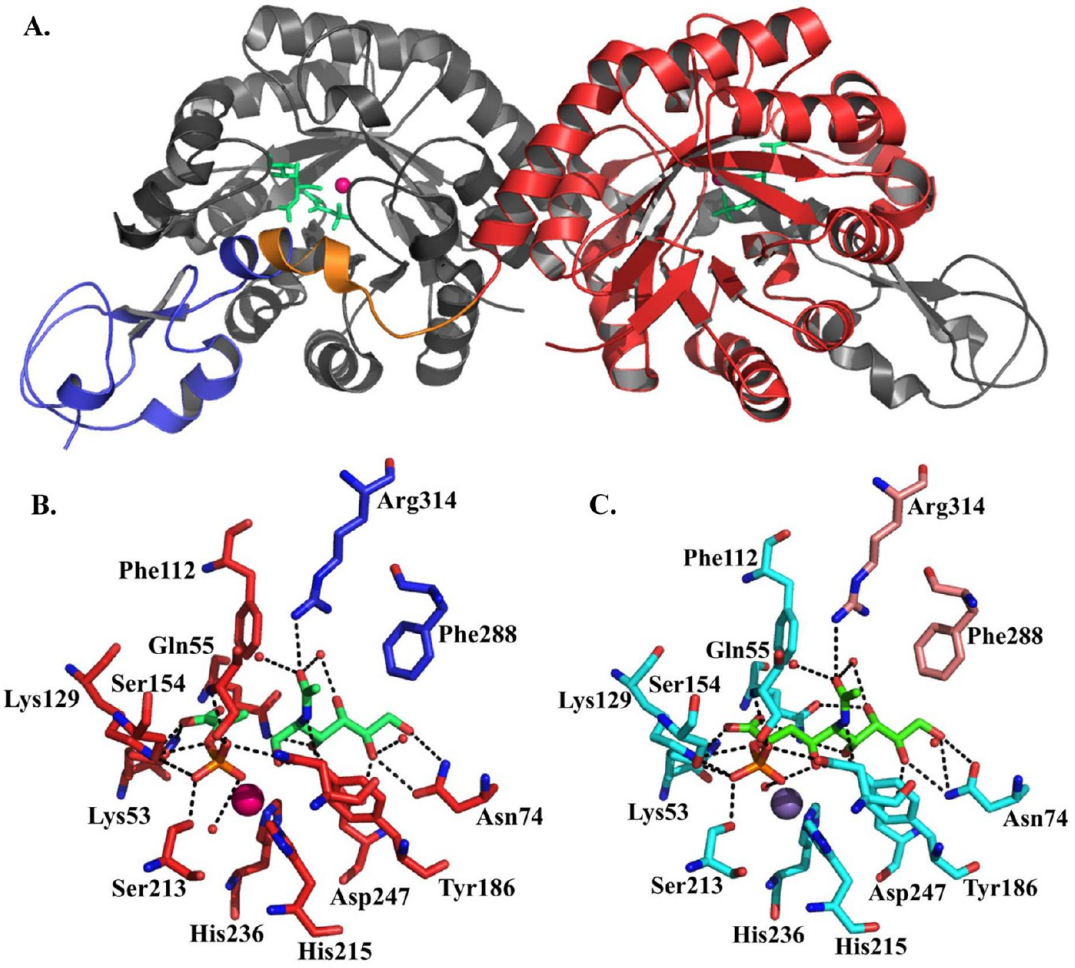

Figure 2. Structure of *Nme*NANAS. (A) The homodimer with the catalytic domain shown in red, linker domain in orange, and AFPL domain in blue. (B) Close up of 1XUZ active site. Residues from catalytic domain shown in red, and residues from AFPL domain in blue. PEP and rManNAc are shown in green and Mn^{2+} in pink. (C) Close up of the 2WQP active site. Residues from catalytic domain are shown in light blue, and residues from AFPL domain are in light pink. Tetrahedral intermediate inhibitor is shown in green and Mn^{2+} is in purple. (PDB code for 2A/B is 1XUZ, for 2C is 2WQP).[1,9]

domain of the opposing monomer, donating one key residue (Arg314) directly into the active site. Arg314 is positioned to form a hydrogen bond with the acetyl oxygen of rManNAc and is thus proposed to interact with the congruent functionality of the natural substrate. Residue Arg314 is also highly conserved in bacterial sialic acid synthases. The importance of Arg314 has been previously implicated in *Streptococcus agalactiae* NANAS where treatment of the enzyme with the Arg modifying reagent phenylglyoxal was found to inhibit catalytic activity.[14]

NANAS is a member of the α-keto acid synthase family and is closely related to both 3-deoxy-D-*arabino*-heptulosonate 7-phosphate synthase (DAH7PS) and 3-deoxy-D-*manno*-octulosonate 8-phosphate synthase (KDO8PS).[18] DAH7PS and KDO8PS catalyze analogous aldol-like condensation reactions between PEP and either erythrose 4-phosphate or arabinose 5-phosphate as part of the shikimate pathway or lipopolysaccharide respectively.[19,20] Although the overall reaction chemistry is similar between each of these three PEP-utilizing aldolases, [9] and all three enzymes adopt a $(\beta/\alpha)_8$ barrel catalytic domain and are considered to share a common evolutionary origin,[18] the AFPL domain of NANAS is a unique decoration that has not been observed in any DAH7PS or KDO8PS.

Arg314 is the only residue of the AFPL domain to contribute directly to the active site of *Nme*NANAS. The combination of its strong interaction with the aldehydic substrate and its high degree of conservation make Arg314 an appealing target for mutagenesis. Herein, we report an investigation into the role of residue Arg314. These studies have revealed that this residue is critical for catalysis by NANAS, playing a vital role in steering

dx.doi.org/10.1021/bi400062c | *Biochemistry* 2013, 52, 2609−2619

Table 1. Mutant Oligonucleotide Primer Sequences

oligonucleotide	sequence (5′-3′)
*Nme*R314K (Fwd)	GAGATAACCTATGGGTTAAAAAACCAGGCAATGGAGACTTCAG
*Nme*R314K (Rev)	CTGAAGTCTCCATTGCCTGGTTTTTTAACCCATAGGTTATCTC
*Nme*R314A (Fwd)	GATAACCTATGGGTTAAAGCGCCAGGCAATGGAGACTTC
*Nme*R314A (Rev)	GAAGTCTCCATTGCCTGGCGCTTTAACCCATAGGTTATC

the aldehyde substrate of NANAS for productive reaction with PEP.

MATERIALS AND METHODS

Cloning, Expression, and Purification of Wild-Type and Mutants. The *neuB* gene from *N. meningitidis* serotype B strain MC58 was amplified from genomic DNA using *Pfu*Ultra DNA polymerase (Agilent). Gene specific nested primers were designed incorporating generic extensions (underlined) for further rounds of nested PCR; F1 (5′-GGCAGCGGCGGC-ATGCAAAACAACAACGA-3′) and R1 (5′-GAAAGCTGGGTGTTATTCAATATCAGT-3′). The product from first round PCR was extended using generic gateway primers (overlapping sequence to first round underlined); F2 (5′-GGGG*ACAAGTTTGTACAAAAAAGCAGGCT*-TCGAAAACCTGTATTTTCAGGGCAGCG GCGGC-3′) which incorporated the attb1 site (in italics) and R2 (5′-GGGGAC*CACTTTGTACAAGAAAGCTGGGT*-3′), which incorporated the attb2 site (in italics). The linear product from second round nested-PCR was cloned into the donor vector pDONR-221 using BP clonase enzyme mix (Invitrogen). Ligated product was subsequently transformed into *Escherichia coli* One Shot TOP10 cells (Invitrogen). Plasmid from transformant was purified using a High Pure Plasmid Isolation kit (Roche), and the *NeuB* gene was successfully sequence verified in the donor vector. LR clonase enzyme mix (Invitrogen) was used to subclone into the destination vector pDEST-17 which encodes an N-terminal His-tag and TEV protease cleavage site.

Variants of *Nme*NANAS were generated by site-directed mutagenesis. The following primers (Table 1) were used to generate mutants using the aforementioned pDEST-17-*Nme*NANAS plasmid as a template.

The vectors bearing the genes of the wild-type and variant proteins were transformed into *E. coli* BL21 (DE3) pBB540/pBB542 cells for expression and purification. Cultures were grown at 37 °C in 1 L of Luria−Bertani (LB) medium supplemented with 100 μg/mL ampicillin, 25 μg/mL chloramphenicol, and 100 μg/mL spectinomycin. Once an A_{600} between 0.5 and 0.6 was reached, overexpression of target protein was induced through the addition of 0.5 mM isopropyl-β-D-thiogalactopyranoside (IPTG), and the culture was further grown overnight at 23 °C. Cells were harvested by centrifugation and resuspended in binding buffer (50 mM potassium phosphate containing 25 mM imidazole and 500 mM NaCl at pH 7.5) prior to lysis by sonication.

The crude lysate was centrifuged at 21000*g* for 35 min, and the supernatant was recovered, filtered, and loaded onto a cobalt affinity Talon (Clontech) column (5 mL). The column was washed with binding buffer, and protein was eluted with elution buffer (50 mM potassium phosphate containing 200 mM imidazole and 500 mM NaCl at pH 7.5). Fractions containing enzyme were pooled together and run through a desalting column eluting with binding buffer to lower the imidazole concentration, before overnight treatment with TEV protease at a 1% mol/mol concentration. TEV treated enzyme was subsequently run through a second Talon column to separate protease and His tag from cleaved enzyme using the same elution conditions as used previously. Untagged enzyme eluted in the flow-through of the second Talon column and was pooled together for size exclusion chromatography (SEC) into buffer containing 30 mM triethanolamine-HCl at pH 7.5. Fractions containing *Nme*NANAS (as determined by gel electrophoresis) were concentrated by ultrafiltration using a 20 mL, 10 KDa MWCO device (Sartorius Stedim), and 100 μL aliquots were flash-frozen with liquid N_2 and stored at −80 °C.

The purification method for enzyme used for the preparation of protein for isothermal titration calorimetry (ITC) with Mn^{2+} was slightly altered to ensure no trace metals were present in the enzyme. This was achieved by treating the SEC buffer with Chelex100 resin (BioRad) and incubating the enzyme with 10 mM EDTA prior to SEC. Analysis of EDTA treated enzyme revealed that this enzyme had approximately 2% activity in the absence of metal.

Crystallization and Refinement of R314K and R314A. Purified R314K at a concentration of 12 mg/mL was crystallized in 1.9 M malate and 10 mM $MnCl_2$ at pH 6.2, and R314A at a concentration of 11.5 mg/mL was crystallized in 1.7 M malate and 10 mM $MnCl_2$ at pH 6.2 using hanging drop vapor diffusion. Hanging drops were 2 μL in size combining 1 μL of protein with 1 μL of reservoir solution, and the total volume of the reservoir solution was 500 μL. Data sets were collected at the Australian Synchrotron using the MX1 and MX2 beamlines. Orthorhombic crystals with a space group of $P2_12_12$ were obtained of both mutants. The structures for both R314K and R314A were solved by molecular replacement using the structure of the wild-type protein (1XUZ).[9] Measured intensities were converted into amplitudes by using TRUNCATE as part of Scalepack2mtz or dtrek2mtz (CCP4).[21] The structure was then solved by performing two rounds of rigid-body refinement (CCP4). Intensity-based refinement was carried out with REFMAC5 (CCP4) following each cycle of structure development from Coot. Water molecules were added automatically following the criterion that they had at least one hydrogen-bonding partner to a protein atom and/or water molecule in the range 2.4−3.2 Å. The final refinement statistics for the structure are given in Table 1. Atomic coordinates and structure amplitudes have been deposited with the PDB under accession codes 4IPJ for R314K and 4IPI for R314A.

A variety of crystallization conditions and soaking conditions were screened to try to obtain crystals of the mutants in the presence of substrates PEP and ManAc (or rManAc). Protein crystallization was screened using Molecular Dimensions Morpheus, Midas, JCSG-*plus*, PACT premier, and ProPlex HT-96 screens; no additional crystallization conditions that yielded crystals of diffraction quality were found. Ligand exchange for the bound malate was trialed, as reported for wild-type NANAS.[1,9] However, under these conditions crystal quality was found to be greatly compromised.

dx.doi.org/10.1021/bi400062c | *Biochemistry* 2013, 52, 2609−2619

Kinetic Assay of Wild-Type, R314K, and R314A. To determine the kinetic parameters of wild-type, R314K, and R314A *Nme*NANAS, the consumption of PEP was monitored at 232 nm ($\varepsilon = 2.8 \times 10^3$ M^{-1} cm^{-1} at 25 °C), and the initial rates of reaction were determined by a least-squares fit. A unit of enzyme activity was defined as the loss of 1 μmol of PEP min^{-1} at 25 °C.

Cuvettes (1 mL) containing 50 mM bis-tris propane (BTP) pH 7.5, 1 mM $MnCl_2$, PEP (varied) and ManNAc (at a range of concentrations) were incubated for 10 min at 25 °C. The enzymatic reaction was initiated by the addition of 5 μL of purified enzyme at a stock concentration of 2.4 mg/mL. Michaelis−Menten steady-state approximations were utilized to determine kinetic parameters with nonlinear fitting in GraFit (Erathicus Software). The concentration of one substrate was kept constant, while varying that of the other and vice versa. To determine apparent $K_{m\ (PEP)}$, ManNAc concentration was held at 30 mM, and the concentration of PEP was varied. To determine apparent $K_{m\ (ManNAc)}$, PEP was kept constant at 1 mM, and ManNAc concentration was varied.

Isothermal Titration Calorimetry (ITC) of wild-type, R314K, and R314A NmeNANAS. The affinity of substrate and metal ions for the wild-type, R314K, and R314A *Nme*NANAS was assessed by ITC using a VP-ITC unit operating at 298 K (MicroCal; GE Healthcare). Prior to use, all solutions were filtered and degassed in a vacuum, and protein concentration was measured by UV absorption ($\varepsilon_{NmeNANAS}$ = 22 270 M^{-1} cm^{-1}). The binding buffer was composed of 30 mM triethanolamine (pH 7.5). To determine $K_{d(Mn)}$, 5 mM $MnCl_2$ was titrated into 70 μM enzyme. To determine $K_{d\ (PEP)}$, 50 mM PEP was titrated into 40 μM enzyme containing a background concentration of 1 mM $MnCl_2$. To determine $K_{d\ (rManNAc)}$, 10 mM rManNAc was titrated into 100−200 μM enzyme containing a background concentration of 1 mM $MnCl_2$ and 1 mM PEP. Titrations were performed with 55 injections of ligand: one 2 μL injection followed by 54 injections of 5 μL. Heats of dilution experiments were measured independently and subtracted from the integrated data before curve-fitting in Origin 7.0 with the standard one-site model supplied by MicroCal.

Modeling of Substrates with Wild-Type, R314K, and R314A. Modeling studies were conducted using software packages from Schrodinger Suite 2011. The structures of the substrate ManNAc were built in Maestro[22] and then prepared using LigPrep.[23] Crystal structure of the wild-type (PDB code 1XUZ) was used for docking. Although the electron density map for the bound rManNAc in this crystal structure is relatively poor, rManNAc is removed prior to docking calculation and thus does not affect the results of the modeling study. The wild-type crystal structure was then prepared using Protein Preparation Wizard in Schrodinger Suite 2011.[24] Because of the malate molecules bound in the active site of R314A and R314K crystal structures, several active site residues adopted slightly different conformations to those observed in the wild-type crystal structure; for example, the active site metal ions of R314A and R314K were shifted in position due to malate molecules coordinating to the metal ions; the residue Tyr186 also showed alternative conformations due to the flexibility of the active site residues in the absence of substrates PEP and ManNAc. Since these residues all have interactions to the substrate bound in the active site, small changes in their positions may affect the outcome of a modeling study, and the differences seen in the modeling results for wild-type and the mutant systems may not reflect only the effect of mutation. Therefore, the enzyme structures of R314K and R314A mutants were made by *in silico* mutation of Arg314 in the prepared wild-type crystal structure (PDB code 1XUZ) to the corresponding Lys and Ala. All other residues in the wild-type structure including the substrate PEP in the active site were retained in the *in-silico*-generated mutant enzymes. The mutant enzymes from *in silico* mutagenesis showed little difference in side chain and backbone positions at residue 314 compared to those in the corresponding crystal structures (Figure S1 in Supporting Information). For all three enzymes, the center of the receptor grid was defined as the centroid of the rManNAc molecule bound in the active site of Chain A; The docking of flexible ManNAc molecule into rigid enzyme receptors of wild-type, R314A and R314K enzymes was conducted in Glide[25−28] with OPLS2005 force field and extra precision (XP) mode. The van der Waals radii of ligand atoms were not scaled. 90 000 poses per ligand were kept for initial docking, and scoring window for keeping initial poses was 5000. The best 1000 poses per ligand were kept for energy minimization with a distance dependent dielectric constant of 2 and a maximum of 5000 conjugate gradient steps. Before any output poses were written out, the poses obtained in the docking calculation were clustered and duplicate poses were discarded if the RMS deviation was less than 0.5 Å and maximum atomic displacement was less than 1.3 Å. This clustering procedure ensures that the output poses were conformationally distinct; as a result different number of output poses was usually written out for different sets of calculations.

In order to assess how closely the output poses from the modeling study resembles the crystallographically observed binding pose of the substrate analogue rManNAc, RMS deviations between poses from modeling study and the crystal structure were measured using the measurement tool in Maestro.[22] The wild-type and mutant receptors used for the modeling study were first superimposed with the wild-type crystal structure, and then the RMS deviations between the modeled poses and the crystal structure of rManNAc were measured in place. Since there are no hydrogen atoms in the original crystal structure, hydrogen atoms in the modeled poses were not included for the calculation of RMS deviations.

RESULTS

Structure of Mutants. In order to assess the role of Arg314 in *Nme*NANAS, two variants of the protein were generated. In the first, Arg314 was substituted for Lys in order to diminish the hydrogen bonding capability of the side chain but preserve some of the functionality of the wild-type protein. For the second variant, Arg314 was substituted for Ala, removing the hydrogen bonding capability of the side chain at this residue completely.

Crystal structures of R314K *Nme*NANAS and R314A *Nme*NANAS were successfully solved to resolutions of 2.15 and 1.75 Å respectively (Table 2). The overall fold of both of the *Nme*NANAS variants was found to be very similar to that of the malate-bound wild-type structure (PDB code 1XUU) with RMS deviations between R314K *Nme*NANAS and R314A *Nme*NANAS and the malate-bound wild-type protein of 0.165 Å and 0.183 Å respectively. The space group and unit cell dimensions are also retained.[9]

Crystals were formed in high concentrations of malic acid (1.7−1.9 M), and as a result bound malate was observed in the active sites of both R314K and R314A. Malate binding was also

Table 2. Crystal Parameters, Data Collection, and Refinement Statistics

	*Nme*NANAS R314K	*Nme*NANAS R314A
A. *Data collection*		
crystal system; space group	$P2_12_12$	$P2_12_12$
unit cell parameters (Å)		
a, *b*, *c*, *α*, *β*, *γ*	58.23, 76.05, 77.67, 90.00, 90.00, 90.00	58.00, 75.80, 77.52, 90.00, 90.00, 90.00
resolution range (outer shell) (Å)	38.00−2.15 (2.2−2.15)	27.16−1.75 (1.8−1.75)
measurements	261,329	481,122
unique reflections	19,392	35,205
redundancy	13.5	13.7
completeness (outer shell) (%)	100.0 (100.0)	100.0 (99.9)
I/σ(outer shell) (I)	15.9 (7.3)	21.7 (5.2)
R_{merge} (outer shell)	0.137 (0.405)	0.106 (0.508)
Wilson *B*-value (Å^2)	13.706	10.119
B. *Refinement*		
resolution (Å)	2.15	1.75
R_{cryst}	0.1739	0.1613
R_{free}	0.2423	0.1972
chain length	351	351
observed number of residues	351	351
water molecules	193	359
other	2	3
mean *B* (Å^2)		
protein	23.0	17.2
water	22.9	23.1
other	29.4	16.9
r.m.s.d. from target values		
bond lengths (Å)	0.0139	0.0072
bond angles (°)	1.370	1.110
dihedral angles (°)	5.690	5.449
Ramachandran		
most favored (%)	97.8	98.0
allowed (%)	2.2	2.0
generously allowed (%)	0	0
disallowed (%)	0	0
PDB entry	4IPJ	4IPI

observed in crystals of wild-type enzyme, and soaking with high concentrations of substrate was required to displace malic acid.[9] Crystals of both variant proteins were soaked for 24 h with 2 M sodium phosphate (pH 6.2), 10 mM $MnCl_2$, 10 mM PEP, and 10 mM rManNAc; however, this treatment resulted in significant physical deterioration of the crystals.

Most active site residues in the variant structures are in identical positions to that for the previously elucidated wild-type structures with either malate or substrates bound (PDB codes 1XUU and IXUZ respectively). In both variant structures the backbone conformation at the site of mutation is retained, and changes in density pertaining to the mutated residue are clearly apparent (Figure S2 in Supporting Information). In the substrate-bound wild-type structure, the hydroxyl group of Y186 is positioned closer to the active site Mn^{2+} ion (hydroxyl is 2.8 Å away from Mn^{2+}), whereas in the malate-bound wild-type structure Y186 is slightly displaced (hydroxyl is 4.5 Å away from Mn^{2+}). Partial occupancy of both conformations for this residue is observed in the structures of R314K and R314A *Nme*NANAS (Figure 3 and Figure S3 in Supporting Information). Malate bound in the active site of R314A is observed in two alternative conformations in both enzyme variants. One of these conformations is similar to that observed in the malate bound wild-type NANAS (Figure 3). There is also a slight change in positioning of Mn^{2+} (1.0 Å toward Y186) for the malate bound structures (including the wild-type structure 1XUU) when compared to the substrate bound wild-type structure (1XUZ), which presumably arises due to the presence of different ligands in the active site. One possible consequence of the substitution of Arg314 for Ala could be the loss of the ability of the protein to exclude water molecules from the active site. A comparison between the wild-type, R314K and R314A *Nme*NANAS crystal structures around the site of mutation indicates that R314A *Nme*NANAS does not bind additional water molecules in the region where Arg314 side chain is missing (Figure S4).

Activity Assay of Mutants. Previously, the use of two different assays has been described in the literature for determining the kinetic parameters of *Nme*NANAS. The first of these is a stopped assay, whereas the second is a continuous assay where NANAS activity is coupled with NANA lyase.[9,29] Here we report the use of a continuous assay that directly monitors the loss of PEP. This assay has been previously described for activity assays of other PEP aldolases such as DAH7PS and KDO8PS.[20,30]

Kinetic parameters for both wild-type and R314K *Nme*NANAS were determined (Table 3). Although catalytically active, an approximately 7-fold reduction in the specificity constant with respect to R314K *Nme*NANAS was observed. This change arises from both a reduction in the k_{cat} (approximately 2-fold) and an elevation in the $K_{m(ManNAc)}$ for R314K *Nme*NANAS in comparison to wild-type *Nme*NANAS. In contrast, $K_{m(PEP)}$ values of R314K variant and the wild-type *Nme*NANAS are quite similar. No loss of PEP was observed with R314A *Nme*NANAS even with the addition of 10-fold excess of enzyme, indicating that this enzyme was unable to catalyze the aldol condensation between PEP and ManNAc.

Isothermal Titration Calorimetry of NANAS Wild-Type and Variants. In order to probe the causes for the loss of activity of the R314A variant of *Nme*NANAS, binding studies were undertaken using isothermal titration calorimetry (ITC). ITC was used to determine the dissociation constants (K_d) for *Nme*NANAS wild-type, and both the R314K and R314A variants of this protein, for both metal and substrates (Table 4 and Figure 4).

To determine the K_d values for metal with wild-type, R314K and R314A *Nme*NANAS, Mn^{2+} was titrated into metal-free enzyme. Mn^{2+} was chosen to investigate metal binding, as it has been previously established as the most activating metal.[17,31] The titration of Mn^{2+} into metal-free enzyme revealed similar affinity of these three enzymes for this metal ion. This is unsurprising given that the mutations made are not proximal to the metal binding site. Titration of PEP into metal-bound enzymes revealed that the K_d values of PEP with respect to R314K and R314A were almost 2-fold greater than those determined for the wild-type enzyme. Interestingly, it was noted that the binding of PEP into *Nme*NANAS wild-type, R314K and R314A was exothermic, and hence a large favorable entropy must be associated with PEP binding (Figure 4D−F).

dx.doi.org/10.1021/bi400062c | *Biochemistry* 2013, 52, 2609−2619

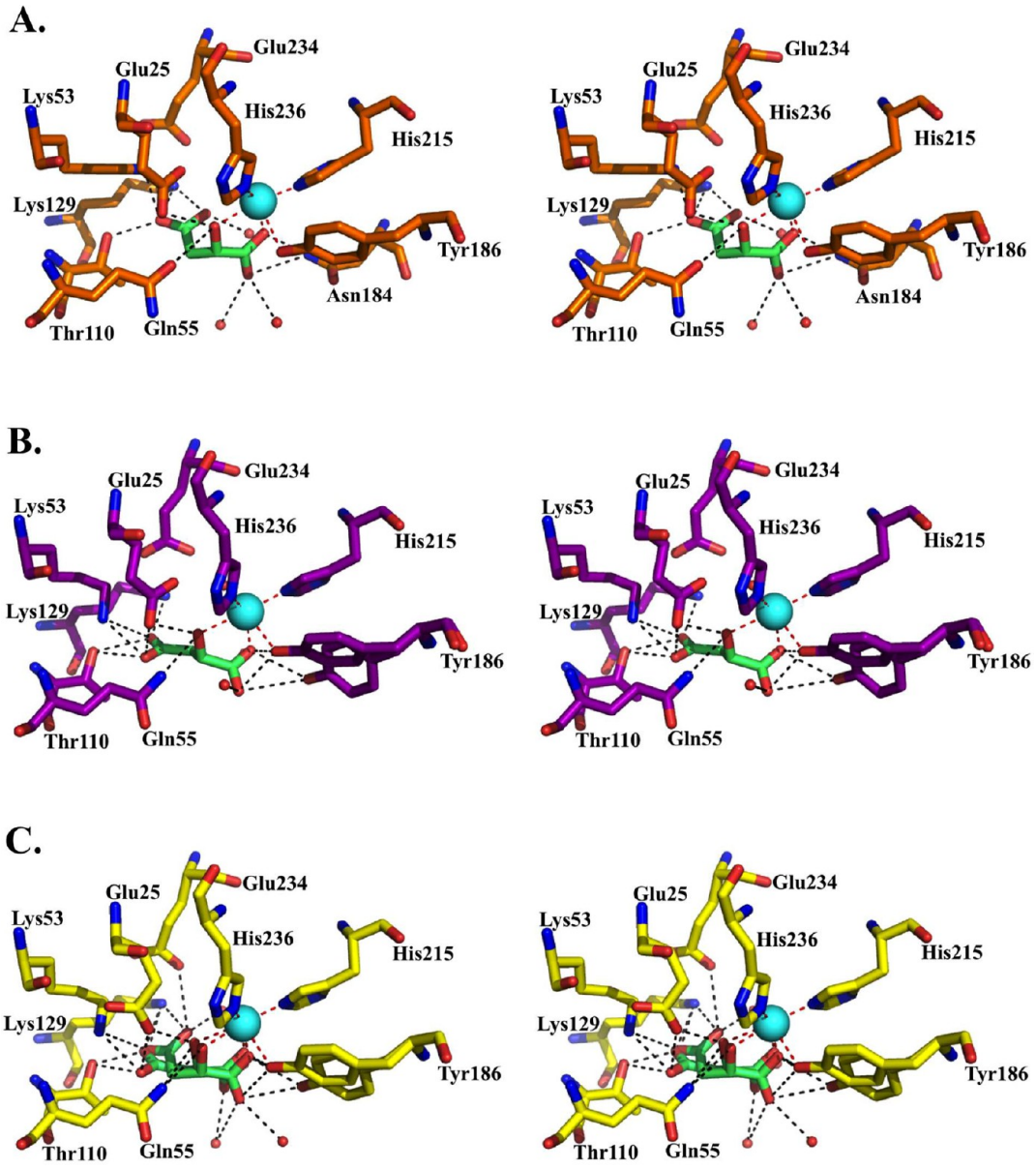

Figure 3. (A) Stereo view of active-site structure of malate-bound *Nme*NANAS wild-type (PDB code 1XUU), residues shown in orange. (B) Active-site structure of R314K NANAS, residues shown in purple. (C) Active-site structure of R314A NANAS, residues shown in yellow. Malate is shown in green and Mn^{2+} is in blue. Hydrogen bonds to malate with distances between 2.0 and 3.4 Å are displayed with black dashed lines, and metal−ligand interactions are displayed with red dashed lines. Note: the side chain of Gln55 in the two mutant structures is flipped compared to that of the wild-type structure. This particular conformation was modeled in the mutant structures as it allows for more reasonable hydrogen bonds with surrounding residues.

Table 3. Kinetic Parameters for Wild-Type and Variants of *Nme*NANAS

	wild-type *Nme*NANAS	R314K *Nme*NANAS	R314A *Nme*NANAS[a]
k_{cat} (s^{-1})	3.1 ± 0.1	1.7 ± 0.1	−
K_m PEP (μM)	28 ± 3	32 ± 3	−
K_m ManNAc (mM)	2.9 ± 0.2	10.5 ± 0.1	−
k_{cat}/K_m ManNAc (s^{-1}/M)	1068 ± 108	162 ± 11	−

[a]Values with − indicates k_{cat} of enzyme is less than 0.004 s^{-1}.

Table 4. ITC Derived Binding Constants for Wild-Type and Variants of *Nme*NANAS

	wild-type	R314K	R314A
K_d Mn^{2+} (μM)	10.6 ± 0.5	13.5 ± 0.4	4.8 ± 0.1
K_d PEP (μM)	219 ± 11	406 ± 12	382 ± 26
K_d rManNAc (μM)	201 ± 16	206 ± 18	377 ± 26

Titration of ManNAc into PEP-free and metal-bound wild-type or variant enzymes did not result in any observable heat changes. However, measurable heat changes were observed when rManNAc was titrated into the metal-bound enzymes with saturating levels of PEP present. Evidence for the binding of rManNAc was not observed in the absence of PEP, demonstrating that a functional binding site for the aldehydic substrate requires PEP to be bound to the protein. The dissociation constants for rManNAc with wild-type and R314A *Nme*NANAS in the presence of metal and PEP were found to

dx.doi.org/10.1021/bi400062c | *Biochemistry* 2013, 52, 2609−2619

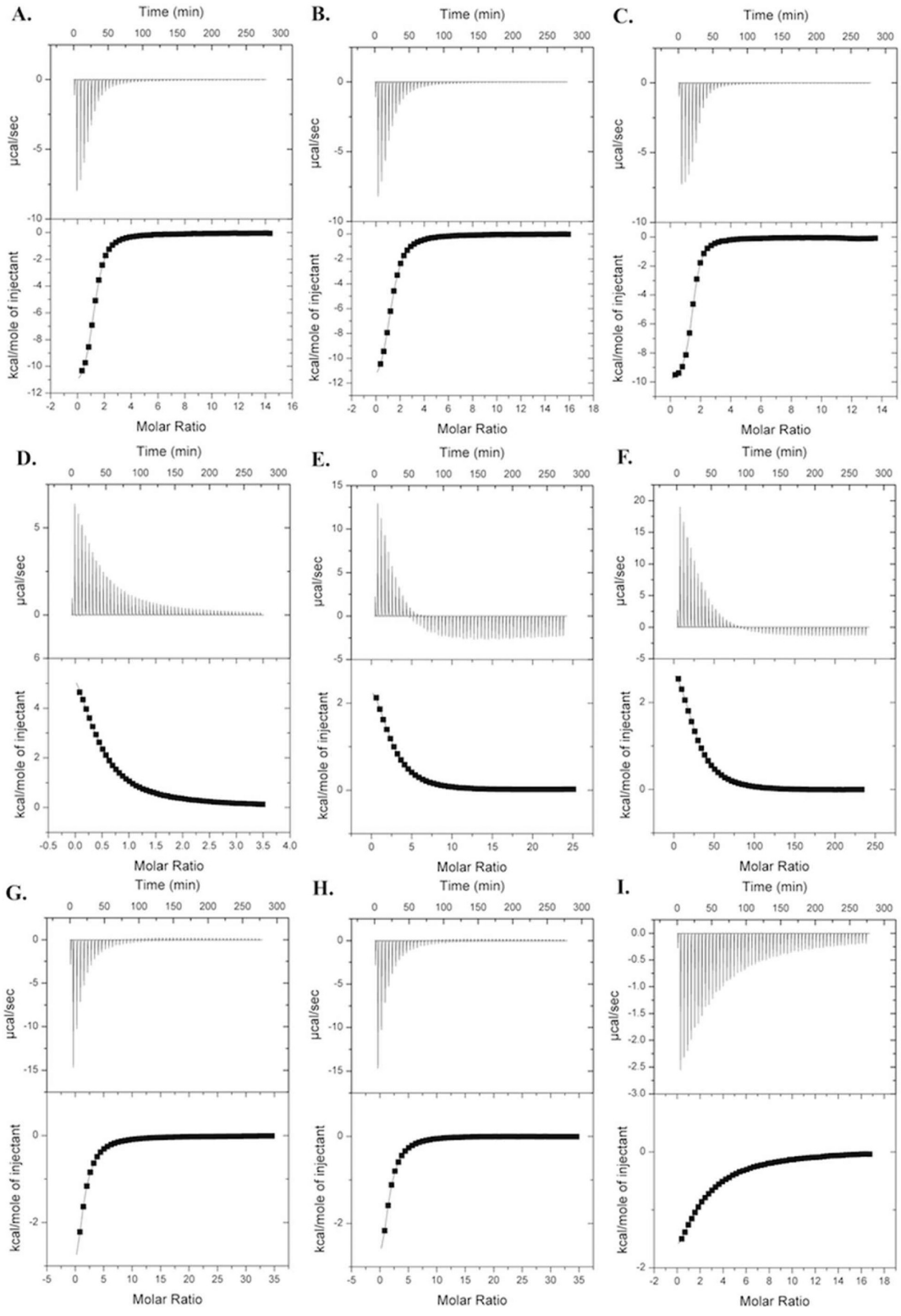

Figure 4. Enthalpy changes measured by isothermal titration calorimetry. (A–C) Mn^{2+} binding to metal-free *Nme*NANAS wild-type, R314K, and R314A respectively. (D–F) PEP binding to metal-bound *Nme*NANAS wild-type, R314K, and R314A respectively. (G–I) rManNAc binding to PEP/metal-bound *Nme*NANAS wild-type, R314K, and R314A respectively.

be similar; however, for the R314A variant, the K_d for rManNAc was significantly greater.

Modeling of ManNAc into Wild-Type and Mutant Active Sites. In the crystal structure of wild-type *Nme*NANAS (PDB code 1XUZ), the substrate analogue rManNAc is bound in the active site.[9] The C1 hydroxyl group of rManNAc that corresponds to the aldehyde of ManNAc is held in position by hydrogen bonds to Tyr186, His236, and a water molecule. The hydroxyl groups on the carbon chain of rManNAc pick up hydrogen bonds with residues Asp247, Gln55, and Asn74. The

dx.doi.org/10.1021/bi400062c | *Biochemistry* 2013, 52, 2609–2619

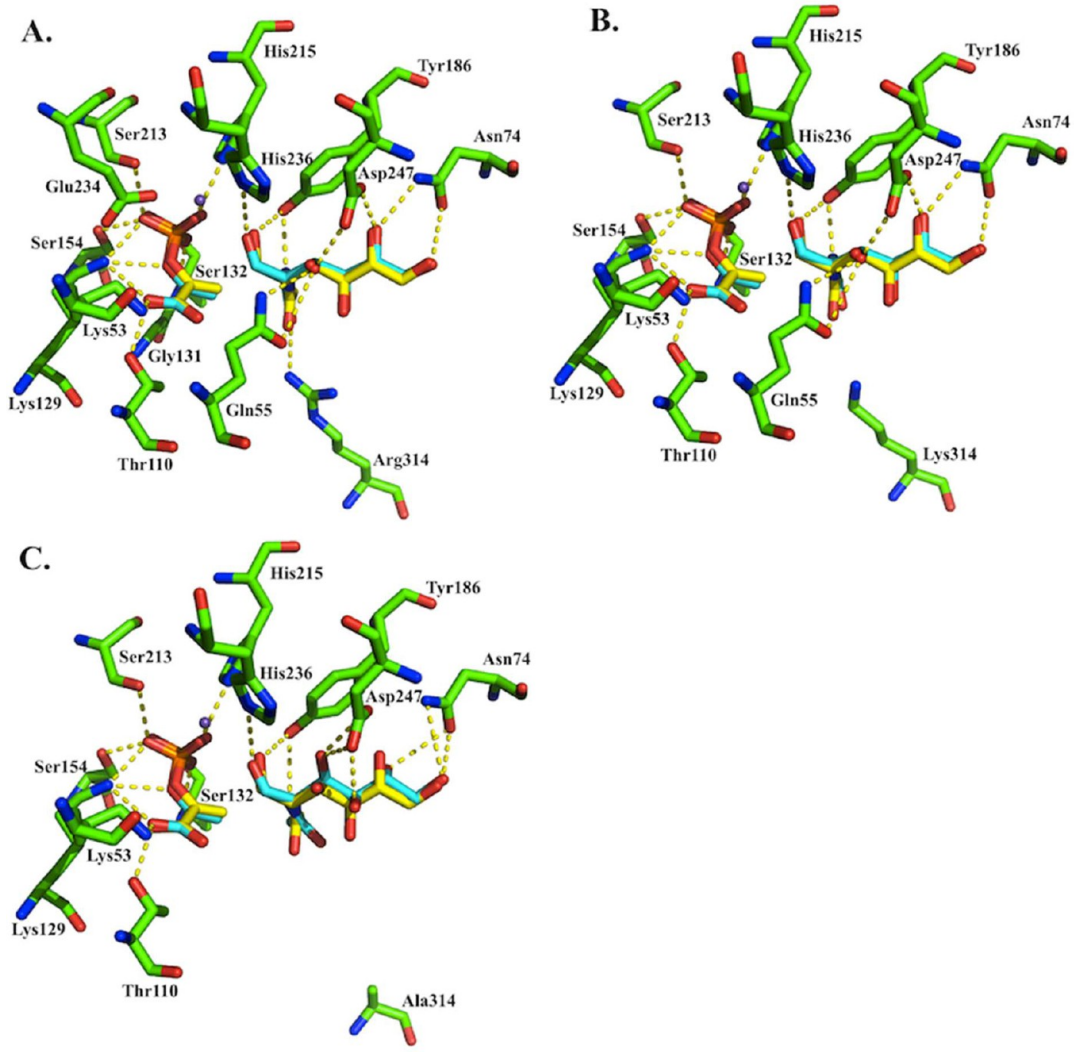

Figure 5. Docking poses of ManNAc in to the enzyme of (A) wild-type, (B) R314K, and (C) R314A, superimposed with the binding poses of PEP and rManNAc from the crystal structure, which are displayed with yellow carbon atoms (PDB code 1XUZ).

side chain of Arg314 mainly interacts with the *N*-acetyl group of rManNAc. In order to investigate the effect of R314K and R314A mutations on the binding mode of substrate ManNAc, molecular modeling studies were conducted.

ManNAc was first modeled into the wild-type active site to confirm that the correct binding pose for this substrate was reproduced in the docking calculation. The modeling study produced a total of 10 possible low energy binding poses for ManNAc in the wild-type enzyme; all of the 10 poses predicted similar positioning of the *N*-acetyl group of ManNAc as that observed for rManNAc in the crystal structure, i.e., with the *N*-acetyl group interacting with Arg314 (Figure S5A in Supporting Information). The distance between the *N*-acetyl carbonyl carbon atoms in the crystal structure and those in the output poses ranges from 0.15 to 0.55 Å (Table S1 in Supporting Information). Each of the output poses was compared to the observed binding mode of ManNAc analogue, rManNAc, and RMS deviations were measured (Table S2 in Supporting Information). The output pose in the wild-type enzyme with the smallest measured RMS deviation closely resembles the binding pose of rManNAc observed in the crystal structure (Figure 5A, Figure S6A), with identical interactions between the substrate and the active site residues predicted. The aldehyde group of ManNAc in this pose is placed with the distance between the aldehyde carbon and PEP C3 being 3.2 Å, and the distance between aldehyde oxygen and the active site metal ion being 2.7 Å, so that the aldehyde group of ManNAc may coordinate to the metal ion for activation. The Bürgi–Dunitz angle of nucleophilic attack of PEP to the aldehyde was measured to be 94.0° in the crystal structure with rManNAc, which is slightly lower than the normal range of 100–110° for Bürgi–Dunitz angles. This possibly arises from the presence of the tetrahedral center of rManNAc in the crystal structure. The Bürgi–Dunitz angle in the modeled pose of ManNAc with the smallest RMS deviation was measured to be 96.8° (the range of Bürgi–Dunitz angles measured from all output poses is provided in Table S3 in Supporting Information). Therefore, the aldehyde group of ManNAc in this pose is held and positioned favorably for reaction to proceed.

Modeling of ManNAc into the R314K mutant enzyme produced seven possible low energy binding poses for ManNAc in R314K, and all of the seven poses predicted similar positioning of the *N*-acetyl group as that observed in the crystal structure (Figure S5B in Supporting Information). The distance between the *N*-acetyl carbonyl carbon atoms in the crystal structure and those in the output poses ranges from 0.17

dx.doi.org/10.1021/bi400062c | *Biochemistry* 2013, 52, 2609–2619

to 0.43 Å (Table S1 in Supporting Information). Following the same procedure as in the wild-type system, the output poses of ManNAc in R314K *Nme*NANAS were compared with the observed binding mode of rManNAc in the crystal structure, and the RMS deviations were measured (Table S2 in Supporting Information). The output pose of ManNAc in R314K *Nme*NANAS with the smallest RMS deviation is still quite similar to that of rManNAc in the crystal structure (Figure 5B, Figure S6B), with all hydroxyl groups adopting the same positions as observed in the crystal structure. The position of the *N*-acetyl group shifted slightly away from Lys314, due to loss of the hydrogen bond caused by the Arg to Lys mutation. However, the aldehyde of ManNAc in R314K enzyme is still positioned in a similar way as that of the best pose in the wild-type enzyme, with the distance between the aldehyde carbon and PEP C3 being 3.2 Å, and the distance between aldehyde oxygen and the active site metal ion being 2.7 Å. The Bürgi−Dunitz angle in this pose is measured to be 97.4°. Therefore, even with the slight shift of *N*-acetyl groups of ManNAc in the R314K enzyme, the position of the ManNAc molecule especially that of the aldehyde group is not affected significantly, so that the reaction may still proceed for the R314K *Nme*NANAS enzyme.

The modeling of ManNAc into the R314A *Nme*NANAS mutant enzyme produced four poses. Although all four poses predicted that the *N*-acetyl groups of ManNAc occupied the same binding site, due to the loss of Arg314 side chain, the *N*-acetyl groups show a more diverse range of positions compared to the wild-type and R314K variant systems (Figure S5C in Supporting Information). The distance between the *N*-acetyl carbonyl carbon atoms in the crystal structure and those in the output poses ranges from 0.14 to 1.32 Å, in comparison to the ranges of 0.15−0.55 Å for the wild-type and 0.17−0.43 Å for R314K *Nme*NANAS (Table S1 in Supporting Information). The output poses were compared to the crystallographically observed binding pose (Table S2 in Supporting Information), and the pose in R314A enzyme with the smallest RMS deviation appears to be very different from the poses found in wild-type and R314K *Nme*NANAS enzymes (Figure 5C, Figure S6C), with hydroxyl groups on C3, C4, and C5 of ManNAc being placed in different positions to that observed in the crystal structure. The R314A mutation also results in some displacement of the *N*-acetyl and aldehyde groups of ManNAc in the model. Specifically, the distance between the aldehyde carbon of ManNAc and PEP C3 is slightly increased (3.3 Å compared to 3.2 Å for wild-type and R314K *Nme*NANAS systems), and the distance between the aldehyde oxygen and the active site metal ion was found to be similarly larger (2.8 Å compared to 2.7 Å in wild-type and R314K systems). The largest difference between the modeled pose in R314A *Nme*NANAS and that in wild-type and R314K systems is in the Bürgi−Dunitz angle, which is unfavorably reduced to 88.2° (compared to 96.8° and 97.4° in wild-type and R314K *Nme*NANAS systems respectively) due to the changes in conformation of ManNAc in the R314A enzyme (Table S3 in Supporting Information). Therefore, it appears that when the side chain functionality of Arg314 is removed through mutagenesis, the enzyme has a diminished ability to correctly position the ManNAc aldehyde group and therefore to enable the reaction to proceed.

DISCUSSION

The AFPL domain of NANAS is a unique decoration within the PEP aldolase family.[9] Arg314 is highly conserved in the AFPL domain of NANAS from different organisms. The crystal structure of *Nme*NANAS in complex with PEP and rManNAc shows that the highly conserved residue Arg314 contributes hydrogen bonding interactions with the *N*-acetyl functionality of rManNAc and hence ManNAc. Mutagenesis was carried out to substitute residue Arg314 of *Nme*NANAS to both Lys and Ala in order to determine its catalytic role.

Crystal structures of both variant enzymes (R314K and R314A) were obtained confirming that there were no significant conformational changes in the active site or overall fold when compared to the wild-type protein. The variant enzyme R314K *Nme*NANAS was found to be catalytically active; however, R314A *Nme*NANAS was not. Kinetic analysis of R314K *Nme*NANAS revealed that the catalytic activity of this variant was compromised, with the enzyme exhibiting a significantly lower $k_{cat}/K_{m(ManAc)}$. While both K_m and k_{cat} are altered, the mutation of Arg314 to lysine has a larger effect on K_m. It is noted that the effect of K_m is not mirrored by changes in K_d as measured from ITC, suggesting that the K_m value contains a kinetic component. The relatively less affected k_{cat} parameter suggests that there may be an alteration in the contributions of different steps in the overall reaction mechanism to the overall rate of reaction. Titration of Mn^{2+} and PEP into the wild-type and variant enzymes demonstrated that the affinity for the catalytically essential metal ion and the PEP substrate was not significantly altered by the mutations, in accordance with the absence of conformational change noted in the structures of the proteins.

ITC experiments revealed that ManNAc was unable to bind to NANAS in the presence of saturating Mn^{2+}; however when the enzyme was saturated with PEP and metal, binding of the nonreactive ManNAc surrogate rManNAc was observed. This observation implies that PEP binding preorganizes the active site for ManNAc binding. This result is somewhat unexpected given that ITC results clearly indicate that PEP binding is entropically favorable. Other examples of binding events with unfavorable enthalpy have been reported previously, and the largely favorable entropy appears to be mostly contributed by a hydrophobic effect.[32] Both R314K and R314A *Nme*NANAS were also found to bind rManNAc consistent with the modeling studies, which suggests that both variant enzymes can accommodate ManNAc in the active site. However, whereas R314K *Nme*NANAS is still active, the R314A variant is not.

Mutation of Arg314 to lysine gave rise to an enzyme with diminished catalytic activity, indicating that the guanidinium functionality of Arg in this position does not play a direct role in catalysis, whereas the Ala was found to be nonfunctional. Observations from the modeling of ManNAc in R314K and R314A *Nme*NANAS strongly suggest that whereas the guanidinium functionality of Arg314 is not critical for the ability to bind ManNAc in the active site per se as demonstrated by ITC it is required for the correct placement of the *N*-acetyl and aldehyde groups of ManNAc to enable reaction with PEP, and so Arg314 facilitates the functional binding mode of ManNAc. There are two major interactions between Arg314 and ManNAc in the wild-type enzyme that may contribute to the correct placement of *N*-acetyl and thus the aldehyde group. The first is a hydrogen bond with the *N*-

acetyl group of ManNAc in the wild-type enzyme, and the other is the electrostatic attraction between the positively charged guanidinium group of Arg314 and the partially negative carbonyl oxygen of the *N*-acetyl group of ManNAc. Mutation of Arg to Ala in R314A *Nme*NANAS results in loss of both the hydrogen bond and the electrostatic interactions between residue 314 and ManNAc, and modeling indicated that although the active site of R314A *Nme*NANAS can still accommodate the ManNAc molecule with a diverse range of conformations, the placement of *N*-acetyl and aldehyde groups were unfavorable for the reaction to proceed. On the other hand, mutation of Arg to Lys in R314K *Nme*NANAS retains the positive charge on the side chain functionality but results in loss of the hydrogen bond, and it appears that R314K can still facilitate the correct placement of the *N*-acetyl group and the aldehyde group to enable reaction with PEP. These findings suggest that the positive charges on the Arg and Lys side chains are likely to be the critical factor for the correct placement of the *N*-acetyl and aldehyde groups of ManNAc for the reaction to proceed and account for the observation that R314K *Nme*NANAS is catalytically active, whereas R314A *Nme*NANAS is not.

In summary, these studies demonstrate that Arg314 of the AFPL domain of *Nme*NANAS is necessary for efficient catalysis. This observation suggests the AFPL domain contributes directly to catalysis, providing key insight into the role played by this extension to the catalytic domain of the sialic acid synthases, an appendage that is unique to this particular family of α-keto acid synthases.

■ ASSOCIATED CONTENT

Ⓢ Supporting Information

This material is available free of charge via the Internet at http://pubs.acs.org.

Accession Codes

The atomic coordinates and structure amplitudes have been deposited with the Protein Data Bank (http://www.rcsb.org/) with the following accession numbers: 4IPI and 4IPJ.

■ AUTHOR INFORMATION

Corresponding Author

*Address: Department of Chemistry, University of Canterbury, Private Bag 4800, Christchurch, New Zealand. Telephone: (+64) 3 364 5682. Fax (+64) 3 364 2110. E-mail emily.parker@canterbury.ac.nz.

Funding

This research was funded by the Maurice Wilkins Centre for Molecular Biodiscovery. The College of Science, University of Canterbury, and the Maurice Wilkins Centre for Molecular Biodiscovery provided a Doctoral Scholarship for D.D.A.J.

Notes

The authors declare no competing financial interest.

■ ACKNOWLEDGMENTS

We would like to thank the MX1 and MX2 beamlines at the Australian Synchrotron and the New Zealand Synchrotron Group for access to the synchrotron.

■ ABBREVIATIONS

AFPL, antifreeze protein like; BTP, 1,3-bis[tris(hydroxymethyl)methylamino]propane; DAH7PS, 3-deoxy-D-*arabino*-heptulosonate 7-phosphate synthase; EDTA, ethylenediaminetetraacetic acid; IPTG, isopropyl β-D-thiogalactopyranoside; ITC, isothermal titration calorimetry; KDO8PS, 3-deoxy-D-*manno*-octulosonate 8-phosphate synthase; LB, Luria–Bertani; ManNAc, *N*-acetyl mannosamine; ManNAc-6-P, *N*-acetyl mannosamine-6-phosphate; MWCO, molecular weight cut off; NANA, *N*-acetylneuraminic acid; NANA-9-P, *N*-acetylneuraminic acid 9-phosphate; NANAS, *N*-acetylneuraminic acid synthase; *Nme*, *Neisseria meningitidis*; PEP, phosphoenolpyruvate; *Pfu*, *Pyrococcus furiosus*; R.M.S, root-mean-square; rManNAc, *N*-acetylmannosaminitol; SEC, size exclusion chromatography; TEV, tobacco etch virus

■ REFERENCES

(1) Liu, F., Lee, H. J., Strynadka, N. C. J., and Tanner, M. E. (2009) Inhibition of *Neisseria meningitidis* sialic acid synthase by a tetrahedral intermediate analogue. *Biochemistry 48*, 9194–9201.

(2) Tanner, M. E. (2005) The enzymes of sialic acid biosynthesis. *Bioorganic Chem. 33*, 216–228.

(3) Angata, T., and Varki, A. (2002) Chemical diversity in the sialic acids and related alpha-keto acids: An evolutionary perspective. *Chem. Rev. 102*, 439–469.

(4) Glaze, P. A., Watson, D. C., Young, N. M., and Tanner, M. E. (2008) Biosynthesis of CMP-*N*,*N*′-Diacetyllegionaminic acid from UDP-*N*,*N*′-Diacetylbacillosamine in *Legionella pneumophila*. *Biochemistry 47*, 3272–3282.

(5) Finne, J. (1985) Polysialic acid - a glycoprotein carbohydrate involved in neural adhesion and bacterial-meningitis. *Trends Biochem. Sci. 10*, 129–132.

(6) Kleene, R., and Schachner, M. (2004) Glycans and neural cell interactions. *Nat. Rev. Neurosci. 5*, 195–208.

(7) Traving, C., and Schauer, R. (1998) Structure, function and metabolism of sialic acids. *Cell. Mol. Life Sci. 54*, 1330–1349.

(8) Hwang, T. S., Hung, C. H., Teo, C. F., Chen, G. T., Chang, L. S., Chen, S. F., Chen, Y. J., and Lin, C. H. (2002) Structural characterization of *Escherichia coli* sialic acid synthase. *Biochem. Biophys. Res. Commun. 295*, 167–173.

(9) Gunawan, J., Simard, D., Gilbert, M., Lovering, A. L., Wakarchuk, W. W., Tanner, M. E., and Strynadka, N. C. J. (2005) Structural and mechanistic analysis of sialic acid synthase *NeuB* from *Neisseria meningitidis* in complex with Mn^{2+} phosphoenolpyruvate, and *N*-acetylmannosaminitol. *J. Biol. Chem. 280*, 3555–3563.

(10) Chou, W. K., Dick, S., Wakarchuk, W. W., and Tanner, M. E. (2005) Identification and characterization of *NeuB3* from *Campylobacter jejuni* as a pseudaminic acid synthase. *J. Biol. Chem. 280*, 35922–35928.

(11) Liu, F., and Tanner, M. E. (2006) *PseG* of pseudaminic acid biosynthesis - A UDP-sugar hydrolase as a masked glycosyltransferase. *J. Biol. Chem. 281*, 20902–20909.

(12) Sundaram, A. K., Pitts, L., Muhammad, K., Wu, J., Betenbaugh, M., Woodard, R. W., and Vann, W. F. (2004) Characterization of *N*-acetylneuraminic acid synthase isoenzyme 1 from *Campylobacter jejuni*. *Biochem. J. 383*, 83–89.

(13) Chen, H., Blume, A., Zimmermann-Kordmann, M., Reutter, W., and Hinderlich, S. (2002) Purification and characterization of *N*-acetylneuraminic acid-9-phosphate synthase from rat liver. *Glycobiology 12*, 65–71.

(14) Suryanti, V., Nelson, A., and Berry, A. (2003) Cloning, overexpression, purification, and characterisation of *N*-acetylneuraminate synthase from *Streptococcus agalactiae*. *Protein Expr. Purif. 27*, 346–356.

(15) Preston, A., Mandrell, R. E., Gibson, B. W., and Apicella, M. A. (1996) The lipooligosaccharides of pathogenic gram-negative bacteria. *Crit. Rev. Microbiol. 22*, 139–180.

(16) Baardsnes, J., and Davies, P. L. (2001) Sialic acid synthase: the origin of fish type III antifreeze protein? *Trends Biochem. Sci. 26*, 468–469.

(17) Hao, J. J., Balagurumoorthy, P., Suryakala, S., and Sundaramoorthy, M. (2005) Cloning, expression, and characterization

of sialic acid synthases. *Biochem. Biophys. Res. Commun. 338*, 1507−1514.
(18) Bravo, I. G., Garcia-Vallve, S., Romeu, A., and Reglero, A. (2004) Prokaryotic origin of cytidylyltransferases and alpha-ketoacid synthases. *Trends Microbiol. 12*, 120−128.
(19) Alm, M., Pietersma, A. L., Schofield, L. R., and Parker, E. J. (2005) Mechanistic divergence of two closely related aldol-like enzyme-catalysed reactions. *Org. Biomol. Chem. 3*, 4046−4049.
(20) Schofield, L. R., Anderson, B. F., Patchett, M. L., Norris, G. E., Jameson, G. B., and Parker, E. J. (2005) Substrate ambiguity and crystal structure of *Pyrococcus furiosus* 3-Deoxy-D-*arabino*-heptulosonate-7-phosphate synthase: An ancestral 3-Deoxyald-2-ulosonate-phosphate synthase? *Biochemistry 44*, 11950−11962.
(21) Bailey, S. (1994) The CCP4 suite - programs for protein crystallography. *Acta Crystallogr. Sect. D: Biol. Crystallogr. 50*, 760−763.
(22) *Maestro*, version 9.2, Schrödinger, LLC, New York, NY, 2011.
(23) *LigPrep*, version 2.5, Schrödinger, LLC, New York, NY, 2011.
(24) *Schrödinger Suite 2011 Protein Preparation Wizard*; Epik version 2.2, Schrödinger, LLC, New York, NY, 2011; *Impact*, version 5.7, Schrödinger, LLC, New York, NY, 2011; *Prime*, version 3.0, Schrödinger, LLC, New York, NY, 2011.
(25) *Glide*, version 5.7, Schrödinger, LLC, New York, NY, 2011.
(26) Friesner, R. A., Banks, J. L., Murphy, R. B., Halgren, T. A., Klicic, J. J., Mainz, D. T., Repasky, M. P., Knoll, E. H., Shelley, M., Perry, J. K., Shaw, D. E., Francis, P., and Shenkin, P. S. (2004) Glide: a new approach for rapid, accurate docking and scoring. 1. Method and assessment of docking accuracy. *J. Med. Chem. 47*, 1739−1749.
(27) Friesner, R. A., Murphy, R. B., Repasky, M. P., Frye, L. L., Greenwood, J. R., Halgren, T. A., Sanschagrin, P. C., and Mainz, D. T. (2006) Extra precision glide: docking and scoring incorporating a model of hydrophobic enclosure for protein-ligand complexes. *J. Med. Chem. 49*, 6177−6196.
(28) Halgren, T. A., Murphy, R. B., Friesner, R. A., Beard, H. S., Frye, L. L., Pollard, W. T., and Banks, J. L. (2004) Glide: a new approach for rapid, accurate docking and scoring. 2. Enrichment factors in database screening. *J. Med. Chem. 47*, 1750−1759.
(29) Warren, L. (1959) Thiobarbituric acid assay of sialic acids. *J. Biol. Chem. 234*, 1971−1975.
(30) Walker, S. R., and Parker, E. J. (2006) Synthesis and evaluation of a mechanism-based inhibitor of a 3-deoxy-D-*arabino*-heptulosonate-7-phosphate synthase. *Bioorg. Med. Chem. Lett. 16*, 2951−2954.
(31) Blacklow, R. S., and Warren, L. (1962) Biosynthesis of sialic acids by *Neisseria meningitidis*. *J. Biol. Chem. 237*, 3520−3526.
(32) Biela, A., Sielaff, F., Terwesten, F., Heine, A., Steinmetzer, T., and Klebe, G. (2012) Ligand binding stepwise disrupts water network in thrombin: enthalpic and entropic changes reveal classical hydrophobic effect. *J. Med. Chem. 55*, 6094−6110.